Journal of Magnetism and Magnetic Materials 489 (2019) 165388

Contents lists available at ScienceDirect

Journal of Magnetism and Magnetic Materials

journal homepage: www.elsevier.com/locate/jmmm

Research articles

Crossover effect of magnetotransport and magnetocaloric effect in $(La_{0.7}Ba_{0.3}MnO_3)_{1-x}/(Al_2O_3)_x$ composites

A.M. Ahmed*, H.F. Mohamed*, A.K. Diab, Esraa Y. Omar

Physics Department, Faculty of Science, Sohag University, 82524 Sohag, Egypt

ARTICLE INFO

Keywords:
Electrical properties
Microstructure
Point defect
Physical properties
Magnetic properties
Magnetocaloric effect

ABSTRACT

Magnetotransport properties and magnetocaloric effect of $(La_{0.7}Ba_{0.3}MnO_3)_{1-x}/(Al_2O_3)_x$ composites have been investigated through their theoretical and experimental studies. The Al_2O_3 addition increases the resistivity, showing up a crossover from 3D Mott to the soft gap variable range hopping (*VRH*). The relative cooling power of LBMO matrix (~98.77 Jkg^{-1}, $H = 2$ T) is approximately 65 percentage of that of pure Gd (*RCP* = 153 Jkg^{-1}, $H = 2$ T). It means to achieve an active magnetic refrigerator employing LBMO will need more than one and half times the volumes of a refrigerant unit consisting of pure Gd. A good concordance is observed as simulated both resistivity and magnetization curves.

1. Introduction

Perovskite manganese oxide $La_{1-x}A_xMnO_3$ (A = Sr, Ca, Ba, or vacancies) has attracted the interest in the last decade due to the discovery of the phenomenon of colossal magnetoresistance (*CMR*) and their potential applications [1–4]. *CMR* material has made a breakthrough in technology due to spin-polarized tunnelling among grain boundaries, opening a new research channel. Many researches have studied *CMR*-insulators composites, such as LSMO/CeO_2 [5], LSMO/ZrO [6], LSMO/NiO [7], LBMO/NiO [8], and NSMO/CrO [9] to clarify the influence of insulator phase on their magnetotransport properties. These studies have exhibited the unconventional low-temperature resistivity behavior is usually governed by spin-dependent tunnelling [10] and the enhanced electron-electron interaction [11] or could be due to factor like the Kondo effect [12,13]. However, the low-temperature resistivity behavior is still under debate. The magnetic material should have two crucial features to possess a large magnetocaloric effect (*MCE*), large spontaneous magnetization (such as in heavy rare-earth metal, Gd) [14], and a sharp change in magnetization around the transition temperature (such as perovskite manganites). Recent studies have been devoted to explore the *MCE* in perovskite manganite. Few researchers have studied the *MCE* in *CMR* material-based insulator. Therefore, we are considering the influence of the insulating Al_2O_3 addition on magnetotransport properties and magnetocaloric effect of $La_{0.7}Ba_{0.3}MnO_3$ composites, as well as simulate both resistivity and magnetization curves based on the representations of the percolation (according to a phase-separated of ferromagnetic (*FM*) and paramagnetic (*PM*) regions) and phenomenological model, respectively. Finally, we offer a comprehensive configuration of the empirical behavior of the compositions under study.

2. Experimental

High-quality single phase polycrystalline $(La_{0.7}Ba_{0.3}MnO_3)_{1-x}/(Al_2O_3)_x$ composite was obtained by conventional solid-solid reaction method. The detailed description of composites preparation can be found in Ref [14]. Structural characterization was performed through X-ray diffraction (*XRD*) with CuK_α radiation at room temperature. The electrical resistivity was measured by a standard four-point method in zero magnetic field and 0.6 Tesla. Magnetic measurements were performed through a vibrating sample magnetometer (*VSM*, EV9 Model). The *MCE* was evaluated through the study of difference of the isothermal magnetic entropy change ΔS_M (*T, H*) at different temperature by [15]

$$\Delta S_M(T, H) = \sum_i \frac{1}{(T_{i+1} + T_i)}[M_{i+1}(T_{i+1}, H) - M_i(T_i, H)]\Delta H \quad (1)$$

To describe the potential of magnetocaloric materials is the relative cooling power (*RCP*) [16], which is defined by

$$RCP = |\Delta S|_{max}\delta T_{FWHM} \quad (2)$$

where $|\Delta S|_{max}$ is the maximum value of magnetic entropy change and δT_{FWHM} is the full width at half maximum of the peak in the entropy change.

* Corresponding author.
E-mail addresses: a.ahmed@science.sohag.edu.eg (A.M. Ahmed), h.fathy@science.sohag.edu.eg (H.F. Mohamed).

https://doi.org/10.1016/j.jmmm.2019.165388
Received 14 April 2019; Received in revised form 21 May 2019; Accepted 30 May 2019
Available online 30 May 2019
0304-8853/

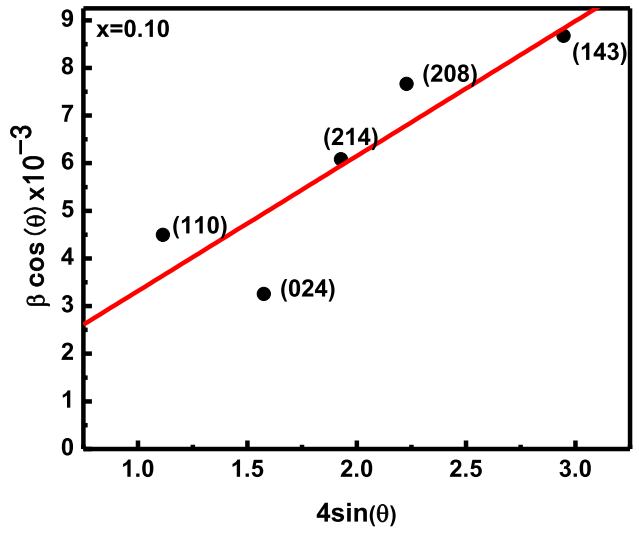

Fig. 1. Plots of $\beta\cos\theta$ vs. $4\sin\theta$ of $(La_{0.70}Ba_{0.3}MnO_3)_{0.90}/(Al_2O_3)_{0.10}$, as an example.

To simulate the variation of magnetization with temperature at constant field by using phenomenological model:

$$M(T, H) = H_{max} = \left(\frac{M_i - M_f}{2}\right) \times [\tan(A(T_C - T))] + BT + C \quad (3)$$

where (M_i/M_f) is an initial/final value of magnetization at *FM-PM* transition as depicted in the inset of Fig. (4),$A = \frac{2(B - S_C)}{M_i - M_f}$, B is the magnetization sensitivity$\frac{dM}{dT}$ at *FM* state before transition, S_C is the magnetization sensitivity $\frac{dM}{dT}$ at Curie temperature T_C, and $C = \frac{M_i + M_f}{2} - BT_C$ The variation of ΔS_M with temperature under adiabatic magnetic field variation from 0 to final H_{max} is available by [17]

$$\Delta S_M = \left[-A\left(\frac{M_i + M_f}{2}\right)\sec^2(A(T_C - T)) + B\right]H_{max} \quad (4)$$

At $T = T_C$, the entropy change reaches its maximum, so the previous equation may be written as the following [17]

$$S_M = \left[-A\left(\frac{M_i + M_f}{2}\right) + B\right]H_{max} \quad (5)$$

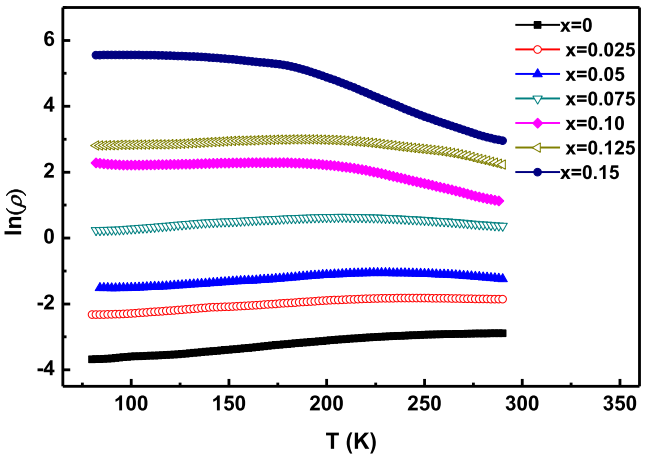

Fig. 2. Temperature dependence of resistivity of $(La_{0.70}Ba_{0.3}MnO_3)_{1-x}/(Al_2O_3)_x$ composites.

3. Results and discussions

The XRD technique of the $(La_{0.7}Ba_{0.3}MnO_3)_{1-x}/(Al_2O_3)_x$ composite has been reported in Ref [14]. Briefly, it showed that the composites are characterized by single-phase rhombohedral ($R\bar{3}C$)structure with no measurable second (Al_2O_3) or impurity phase. The lattice distortion is represented by Goldschmidt tolerance factor $t = d_{A-O}/\sqrt{2}d_{B-O}$ (where d_{A-O}, and d_{B-O}) is the bond length of La/Ba-site and Mn-site, respectively). If t is close to unity, the lattice structure is defined as cubic perovskite; for $0.90 < t < 1$ the structure transforms to the rhombohedral and then to orthorhombic structure for $t < 0.90$. In these composites, the tolerance factor (t) increases up to x = 0.075 wt% then decreases with further Al doping, leading to a transformation in the crystal structure to low symmetry. The average crystallite size [$\langle D_{WH}\rangle$ (nm)] and the strain $\varepsilon = \Delta d/d$ can be estimated from the Williamson–Hall plots [18] through the following expression

$$\beta\cos\theta = \frac{K\lambda}{D} + 4\varepsilon\sin\theta \quad (6)$$

where β, K, λ, ε, θ are the full width at half maximum (*FWHM*), the grain shape factor, the X-ray wavelength, micro-strains (includes the effects of structural defects such as dislocations, stacking faults, twin boundaries and intergrains), and the Bragg diffraction angle, respectively. β must be corrected from the diffractometer contribution by subtracting the value of full-width at half-maxima (β_o) corresponding to

Table 1
Crystal structure, Transition temperature (T_{ms}), Curie temperature (T_c), Maximum entropy change $|\Delta S|_{max}$ and Maximum entropy change (*RCP*) for $(La_{0.70}Ba_{0.3}MnO_3)_{1-x}/(Al_2O_3)_x$ composites.

$(La_{0.70}Ba_{0.3}MnO_3)_{1-x}/(Al_2O_3)_x$	0	0.025	0.05	0.075	0.1	0.125	0.15
Crystal structure							
Tolerance factor 't'	0.9117	0.927695	0.9473	0.9473	0.9295	0.9213	0.9095
Average crystallite size $\langle D_{WH}\rangle_{nm}$, Williamson-Hall	29.61	37.98	33.22	36.17	33.33	32.2	28.57
Strain × $10^{-4}(\varepsilon)$ %	4.76	8.16	21	28.3	21.9	19.8	17.4
Electrical and magnetic properties							
$T_{ms\ (H=0)}$(K)	318	248	230	208	172	196	98
$T_{ms\ (H=0.6T)}$(K)	324	252	244	214	180	198	104
$T_{c\text{-magnetization}}$(K)	308	–	308	–	306	–	306
$\lvert\Delta S\rvert_{max}$[J/Kg.K] *at H(= 3T)*	2.344	–	2.18		2.1	–	2
RCP[J/Kg] *at H(= 3T)*	118.31		114.45		113.69		102.74

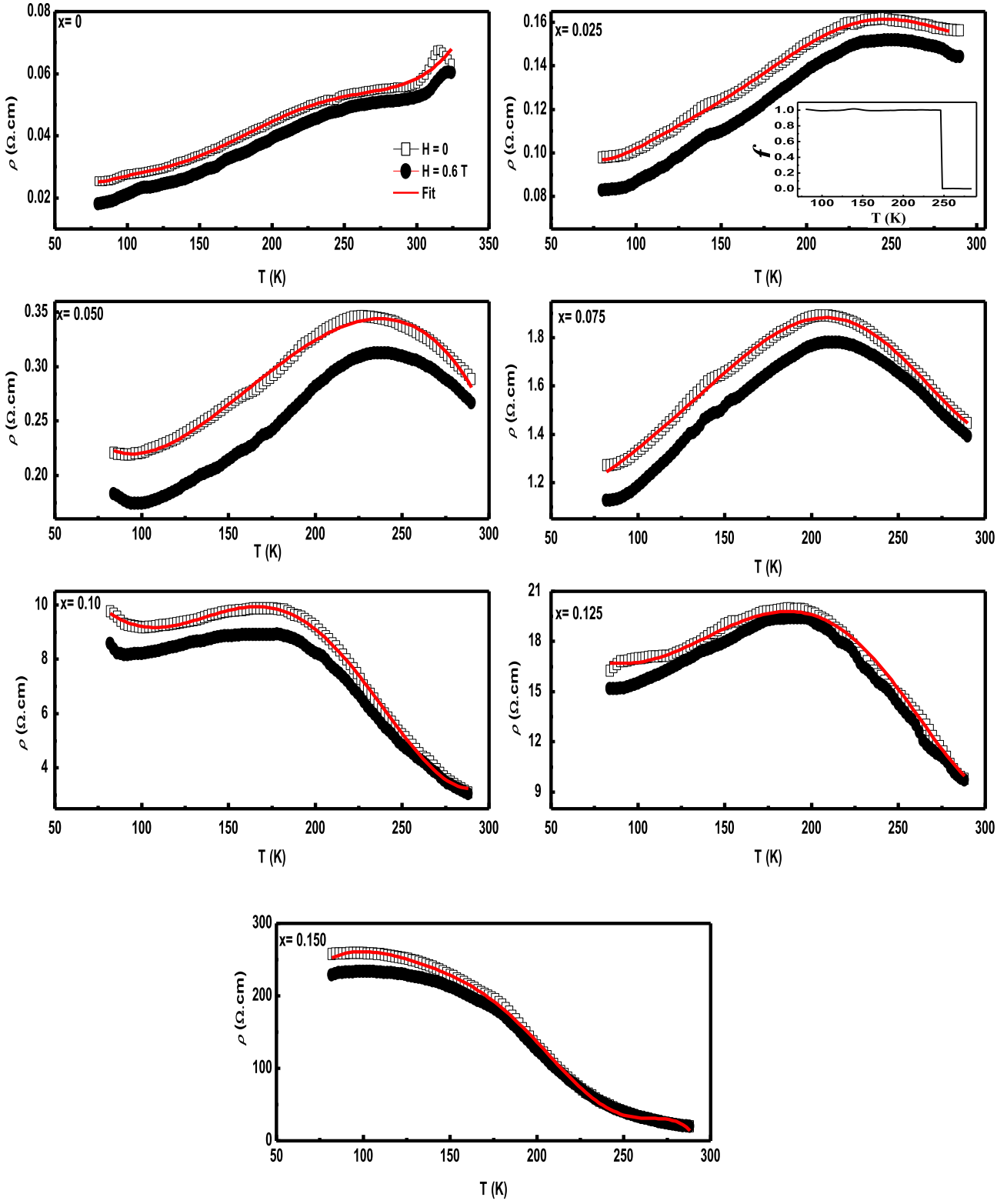

Fig. 3. Electrical resistivity (ρ) as a function of temperature of $(La_{0.70}Ba_{0.3}MnO_3)_{1-x}/(Al_2O_3)_x$ composite at zero and 0.6 T magnetic field. The solid line represents best fit to Eq. (5). The inset shows the temperature dependence of ferromagnetic phase volume fraction of x = 0.025, as an example.

Table 2
Parameters estimated from the best fit to Eq. (9) of the electrical transport data of $(La_{0.70}Ba_{0.3}MnO_3)_{1-x}/(Al_2O_3)_x$ composites.

$La_{0.70}Ba_{0.3}MnO_3)_{1-x}/Al_2O_3)_x$	0	0.025	0.05	0.075	0.10	0.125	0.150
ρ_o(Ω.cm)	1.690	4.097	13.3	89.79	808.002	1539.7	101175.28
ρ_e(Ω.cm $K^{1/2}$)	0.226	0.594	1.79	12.55	116.57	244.72	2,262,477
ρ_s(Ω.cm)	0.833	2.049	6.40	44.34	404.70	828.211	64215.84
ρ_P($\times 10^{-13}$ Ω.cm K^5)	7.927	21.88	132	861.9	12,987	23,500	146,000
ρ_2($\times 10^{-6}$ Ω.cm K^2)	17.76	53.2	154	1070	1126	2455	39,948
$\rho_{4.5}$($\times 10^{-12}$ Ω.cm $K^{4.5}$)	18.38	65.8	269	1765	24,833	47,200	231,280
n_{FM}	4.5	4.5	4.5	4.5	4.5	4.5	4.5
U_o/k_B(K)	1690	5580	21,300	25,100	6850	9040	12,100
E_a/k_B(K)	913.48	1040.92	192.17	206.27	429.64	726.98	2500.6
T_o(x10^5k)	–	0.00274	0.13	0.20	29.54	37.68	13.48
n_{PM}	1	4	4	4	4	2	2

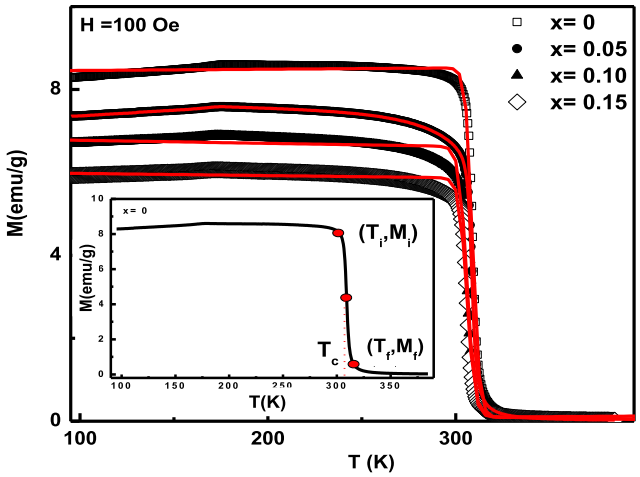

Fig. 4. The experimental (symbols) and calculated (solid lines) magnetization as a function of temperature of $(La_{0.70}Ba_{0.3}MnO_3)_{1-x}/(Al_2O_3)_x$ composites. The inset depicts temperature dependence of magnetization under constant applied field.

a standard sample (LaB_6) from at respective Bragg peaks ($\beta = \sqrt{\beta_o^2 - \beta_{LaB6}^2}$) [19]. After plotting β cosθ vs. 4 sinθ (Fig. 1), the obtained values of the average crystallite size and microstrain are summarized in Table 1. The crystallites size $\langle D_{WH}\rangle$ is larger than that estimated by the Scherrer's equation $\langle D_{SC}\rangle$ that is because the broadening effect due to strain is completely excluded in the Debye–Scherer technique [20]. It is possible to confirm that Al^{3+} is being pushed out towards the grain boundary by the $\varepsilon = \Delta d/d$ values. The $\varepsilon = \Delta d/d$ values larger than 10^{-3} for maganites with many defects, while is lower than 5×10^{-4} for manganites with very few defects [21–23]. The resultant $\Delta d/d$ values of composites varied from 4.7 to 28.3 $\times 10^{-4}$ by adding the non-magnetic Al_2O_3 phase.

Fig. 2 shows the electrical resistivity (ρ) as a function of temperature (T) in zero magnetic fields of the $(La_{0.7}Ba_{0.3}MnO_3)_{1-x}/(Al_2O_3)_x$ composites. As anticipated, the zero field resistivity increases monotonously and the metal-semiconductor transition $(T_{ms}) = \begin{cases} metal, \frac{d\rho}{dT} < 0 \\ semiconuctor, \frac{d\rho}{dT} > 0 \end{cases}$ is shifted successively towards lower temperatures with the increasing Al content (Table 1). The high resistivity of these composites and the alteration of the transition temperature T_{ms} are related to the influence of the additive aluminium on the electron transport channel in the composites. In the LBMO matrix, the electrical transport is occurred through the direct contact between the LBMO grains. Whilst the rest of the composites, there are two kinds of conduction channels connected in parallel in the *FM*-$(LBMO)_{1-x}$/Insulator-$(AlO)_x$ composite [6,8,9]. One is related to the *FM*-(LBMO) grains and the other is related to the I-(AlO) grains. The Al_2O_3, are mostly disturbed at the grain boundaries and on the surface of LBMO grains, acting as a barrier to blocking electron transport, and resulting in the increment of their resistivity. Thereby, this confirms that the T_{ms} is extrinsic property and is strongly depends on the microstructure.

Fig. 3 shows the electrical resistivity in the effect of magnetic field application. The magnetic field application diminishes the resistivity over all temperature range due to spin order the minor carriers scattering, which leads to the negative magnetoresistance. It has more effect at low temperatures and at the transition temperature region. The T_{ms} is shifted slightly to higher temperature due to the alignment of Mn spins that causes the enhancement of the *FMM* (ferromagnetic metal) state. We used a percolation approach to understand the magneto-transport mechanism [24], which is based on the competition between *PM* and *FM* regions. According to Li [24], the resistivity in the whole temperature range may express as follows:

$$\rho(T) = f\rho_{FM} + (1 - f)\rho_{PM} \tag{7}$$

where f and $(1 - f)$ are the volume fractions of *FM* and *PM* phases, respectively. The f function of both phases well satisfies the Boltzmann distribution given as

$$f = \frac{1}{1+\exp\left(\frac{-U_0\left(1-\frac{T}{T_C^{mod}}\right)}{k_B T}\right)} \tag{8}$$

Then the total resistivity dependence on the temperature can be written as:

$$\rho(T) = \left(\frac{1}{1+\exp\left(\frac{-U_0\left(1-\frac{T}{T_C^{mod}}\right)}{k_B T}\right)}\right)\left(\rho_o + \rho_e T^{\frac{1}{2}} - \rho_s \ln T + \rho_{Ph} T^5 + \rho_2 T^2 + \rho_{n_{FM}} T^{n_{FM}}\right)$$

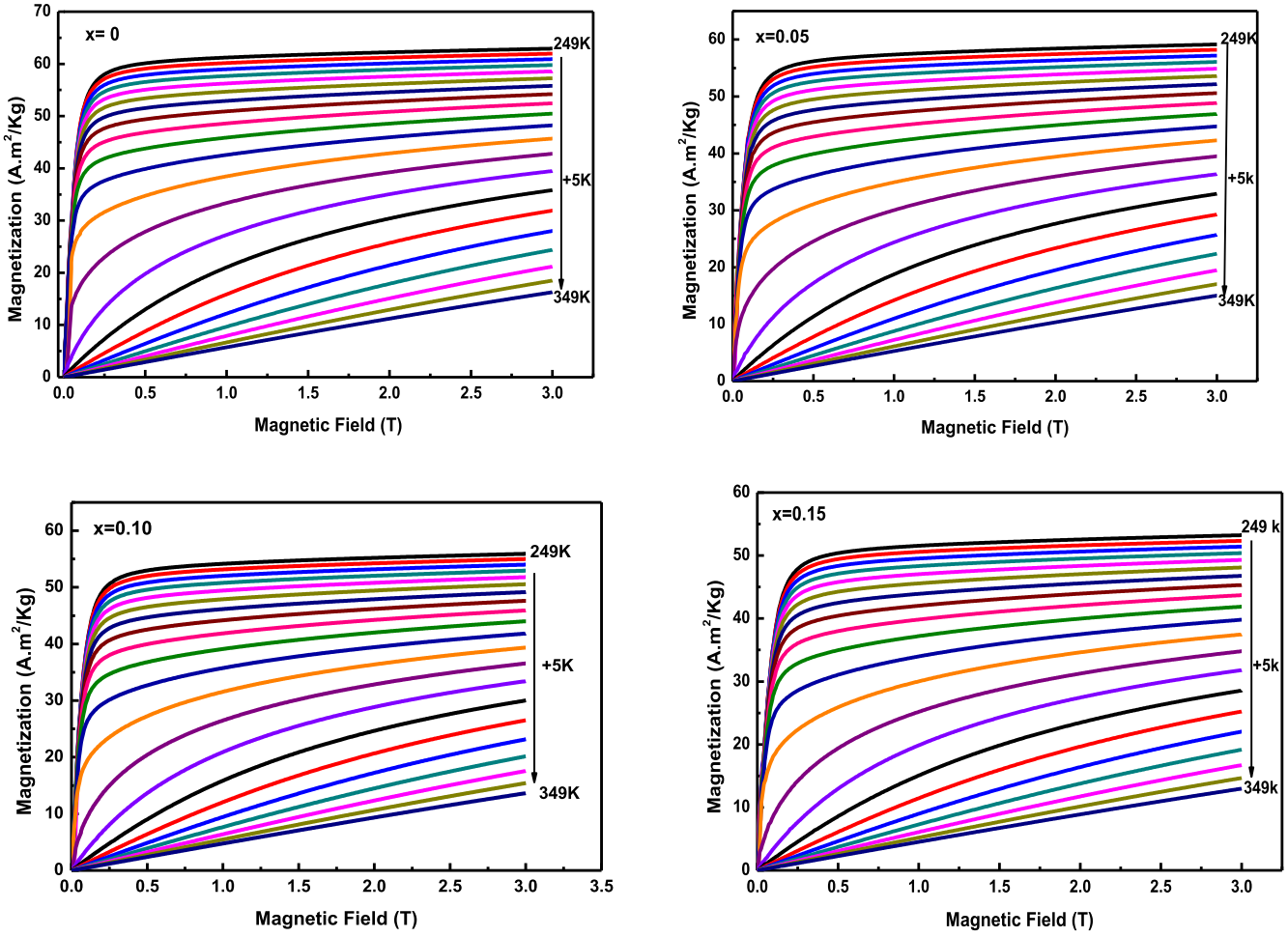

Fig. 5. Isothermal specific magnetization M(H) curves for $(La_{0.70}Ba_{0.3}MnO_3)_{1-x}/(Al_2O_3)_x$ composites.

$$+\left(\frac{\exp\left(\frac{-U_o\left(1-\frac{T}{T_C^{\mathrm{mod}}}\right)}{k_BT}\right)}{1+\exp\left(\frac{-U_o\left(1-\frac{T}{T_C^{\mathrm{mod}}}\right)}{k_BT}\right)}\right)\left(\rho_{n_{PM}}T\ \exp\left(\frac{E_a}{k_BT}\right)^{\frac{1}{n_{PM}}}\right) \tag{9}$$

where ρ_o is the residual resistivity ($T = 0$ K), $\rho_e T^{\frac{1}{2}}$ is attributed to contributions from *e-e* (electron-electron) interactions, $\rho_s$lnT is related to Kono-like spin dependent scattering, $\rho_{Ph}T^5$is due to e-ph (electron-phonon) interactions, $\rho_2 T^2$ indicates e-e scattering $\rho_{n_{FM}}T^{n_{FM}}$, is the physical signification depends on n value (n = 2.5, 4.5) at FM region, T_C^{mod} is *FM–PM* transition temperature used in this approach, U_o is the energy difference in temperature below T_{ms} (metal-semiconductor transition), $\rho_{n_{PM}}T^{\frac{1}{n_{PM}}}$is the physical signification depends on n value (n = 1, 2, 3, 4) at PM region and E_a is activation energy.

Fig. 3 depicts the fitted (red line) and the experimental data of ρ(*T*) curve in zero field of $(La_{0.7}Ba_{0.3}MnO_3)_{1-x}/(Al_2O_3)_x$ composites. The best-fitting parameters are summarized in Table 2. Furthermore, the temperature dependence of the *f* fractions of *FM* phase in zero field is illustrated in the inset of Fig. 3 (as an example x = 0.025). When the temperature is considerably below T_C, *f* is close to 1, which means the phase is completely *FM*, while by increasing the temperature *f* decreases and tends to zero, which attributed completely PM phase transformation. It is noteworthy that this approach is suitable to explain the magnetotransport mechanism of composites. From the obtained fitting parameters, the increment in ρ_2 (arises due to the electron-electron scattering) and $\rho_{4.5}$ (arises due to the electron-magnon scattering) could be ascribed to the increase in electron spin fluctuations with the increase in Al content. The terms ρ_0 and ρ_s give higher value than other parameters, so it is deduced that the resistivity in the ferromagnetic region may be the residual resistivity (adding Al content increases grain boundary), electron–electron interaction and Kondo-like spin-dependant scattering are more effective on the resistivity in the ferromagnetic region. In addition, $\frac{1}{n_{PM}}$ value in the paramagnetic region increases from $\frac{1}{4}$ to $\frac{1}{2}$ as the Al content increases, thereby indicating there is a crossover from the 3D Mott to the soft gap variable range hopping (*VRH*).

Fig. 4 shows the temperature dependence of dc magnetization *M* (*T*)

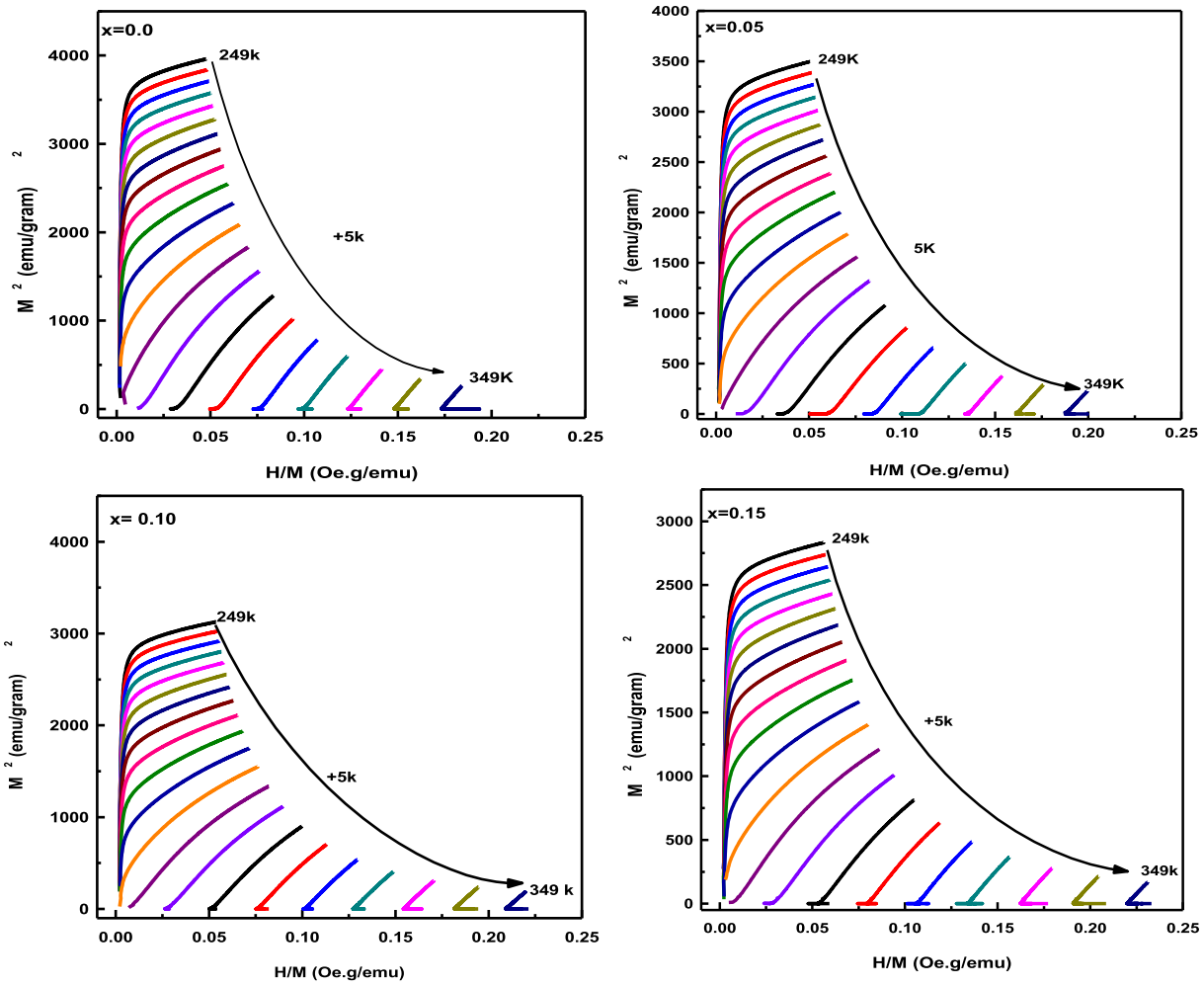

Fig. 6. M^2 versus $\mu_0 H/M$ determined from the magnetization isotherms for $(La_{0.70}Ba_{0.3}MnO_3)_{1-x}/(Al_2O_3)_x$ composites.

plots measured in zero field-cooling (*ZFC*) regimes at 100 Oe applied magnetic field. It can be seen the $(LBMO)_{1-x}/(AlO)_x$ composites show FM-PM transition at T_C. The value and transition width of magnetization decreases with increasing Al concentration. These declines are expected and are attributed to extra grain boundaries and the decrease in the volume fraction of ferromagnetic LBMO, leading to reduction of magnetization. Furthermore, this confirms the correlation between the width of magnetization transition and microstrain. The isothermal magnetization curves of $(LBMO)_{1-x}/(AlO)_x$ composites x = 0, 0.05, 0.10 and 0.15 were measured and shown in Fig. 5. There is a rapid increase in magnetization curves below T_c at $H < 0.5$ T then tends to saturate at $H > 0.5$ T, which confirms the ferromagnetic behavior. Furthermore, above T_c the magnetization increases linearly with increasing the magnetic field, as the typical behavior of paramagnetism. The large variation of magnetization around T_c is attributed to the large magnetic entropy change (ΔS_M). To find the nature of the magnetic transition (first or second order), Arrott plots (M^2 versus $\mu_0 H/M$) are depicted in Fig. 6. The obtained results clearly illustrate a positive slope for the complete M^2, which confirm the second order phase transition [25]. Fig. 7 shows the temperature dependences of ΔS_M (*T, H*) at various strengths of magnetic field from $\mu_0 H$ of 1 T to 3 T, for $(LBMO)_{1-x}/(AlO)_x$ composites. It is observed that ΔS_M shows negative values with a maximum near T_C. This maximum increases and is shifted towards higher temperature with the increase in the applied magnetic field, indicating ΔS_M dependence on the magnetic field strength. The width of ΔS_M is broad in all composites due to the second-order nature of the phase transition. The ΔS_M value decreases with increasing Al content and its highest value is 2.344(J/kg.K) at $H = 3$ T for the LBMO matrix (Table 1). Fig. 8 illustrates the *RCP* values for all composites. The *RCP* increases with the Al content and reaches a maximum value of 118.31 Jkg^{-1} for the LBMO matrix at 3 T-applied magnetic field. As shown in Fig. 8 the *RCP* value of matrix LBMO (~98.77 Jkg^{-1}, $H = 2$ T) is approximately 65 percentage of that of pure Gd (*RCP* = 153 Jkg^{-1}, $H = 2$ T) [26]. It means to achieve an active magnetic refrigerator employing LBMO will need more than one and half times the volumes of a refrigerant unit consisting of pure Gd.

Finally, as evidenced in Figs. 4 and 9 the fitting of the M (T) and ΔS_M (*T*) measurements of our composite (LBMO/AlO) based on this phenomenological model (Eq. (3)) shows a good match between theoretical and experimental result. The best fit-parameters are summarized in Table 3.

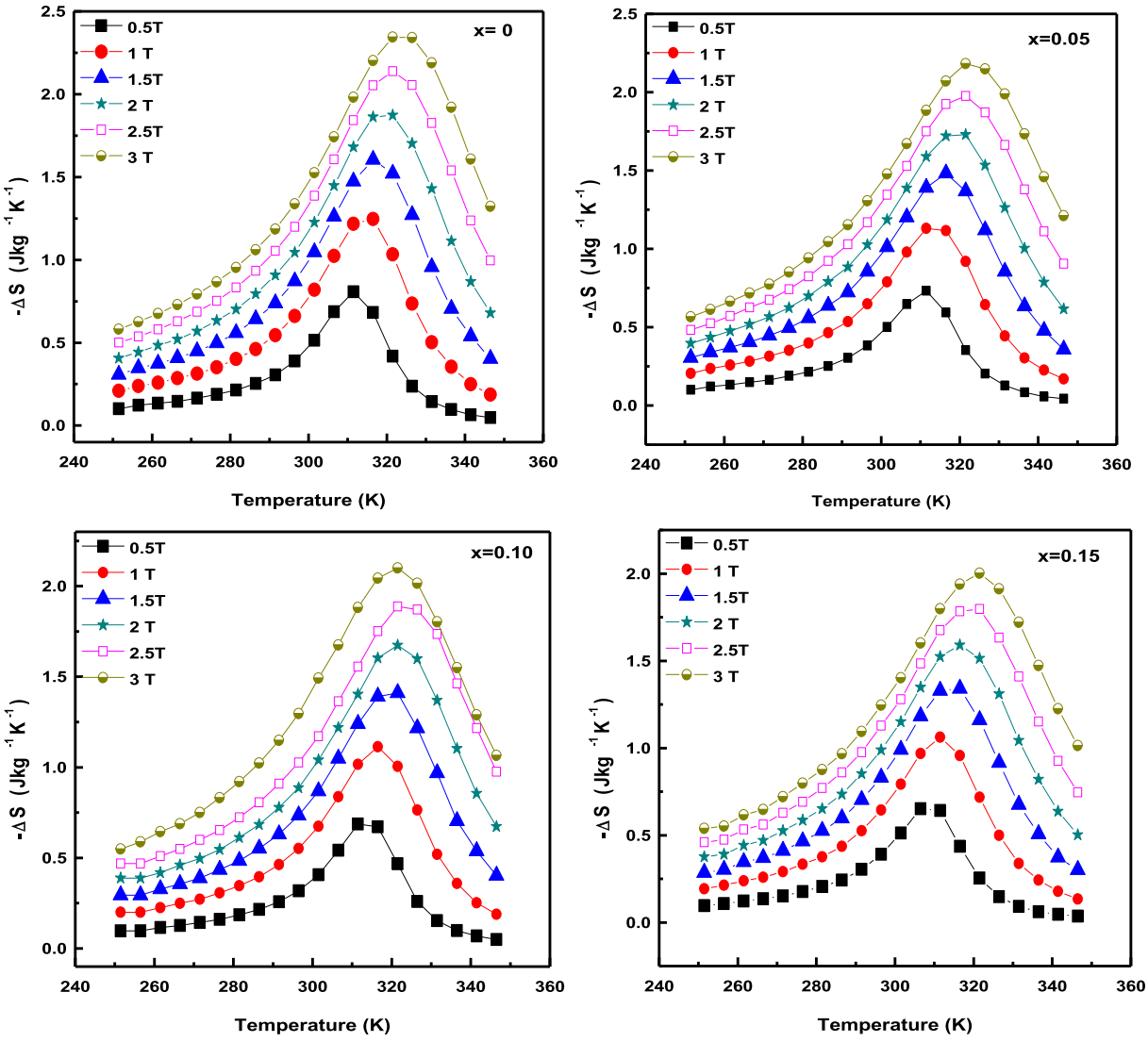

Fig. 7. Magnetic entropy change, $(-\Delta S_M)$, versus temperature for $(La_{0.70}Ba_{0.3}MnO_3)_{1-x}/(Al_2O_3)_x$ composites at different magnetic field.

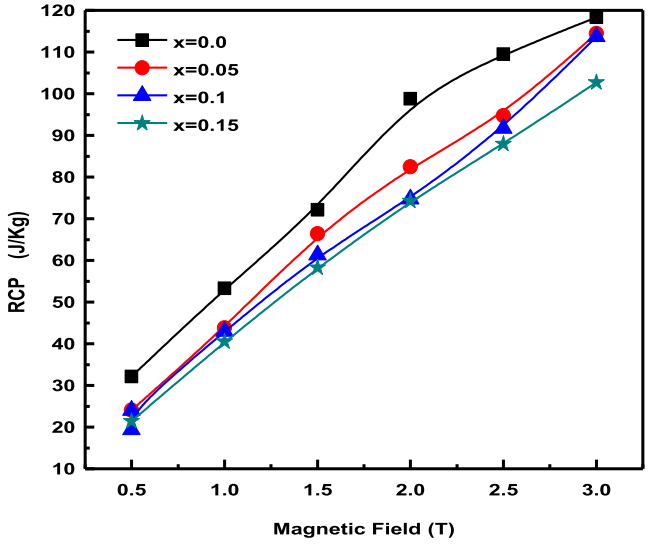

Fig. 8. Relative cooling power values, *RCP* as a function of applied magnetic field (*H*) for$(La_{0.70}Ba_{0.3}MnO_3)_{1-x}/(Al_2O_3)_x$.

4. Conclusion

We presented results of a comprehensive investigation of the structural, magnetotransport properties and magnetocaloric effect of $(La_{0.7}Ba_{0.3}MnO_3)_{1-x}/(Al_2O_3)_x$ composites with x = 0 to 0.15 wt% step 0.025. Structural analysis reveals that the composites are still a single-phase rhombohedral $(R\bar{3}c)$ structure with no measurable impurity, while the rhombohedral distortion after composite x = 0.10 wt% increases. Electrical measurements show the resistivity increases and the metal-semiconductor transition T_{ms} shifts towards lower temperatures with increasing Al content. Based on the percolation model, we have successfully fitted the resistivity curve in the whole temperature range, and this model is suitable to explain magnetotransport mechanism of composites. Notably, there is a crossover from 3D Mott to the soft gap VRH ($\frac{1}{n_{PM}}$, $n_{PM} = 2$) in the paramagnetic region. Magnetic properties exhibit a *FM–PM* transition with increasing temperature. The ΔS_M value decreases with increasing Al content and its highest value of 2.344(J/kg.K) at $H = 3\ T$ for the LBMO matrix. The *RCP* decreases with the Al content and reaches a maximum value of 118.31 Jkg^{-1} for the LBMO matrix at 3T-applied magnetic field. The *RCP* value of LBMO matrix

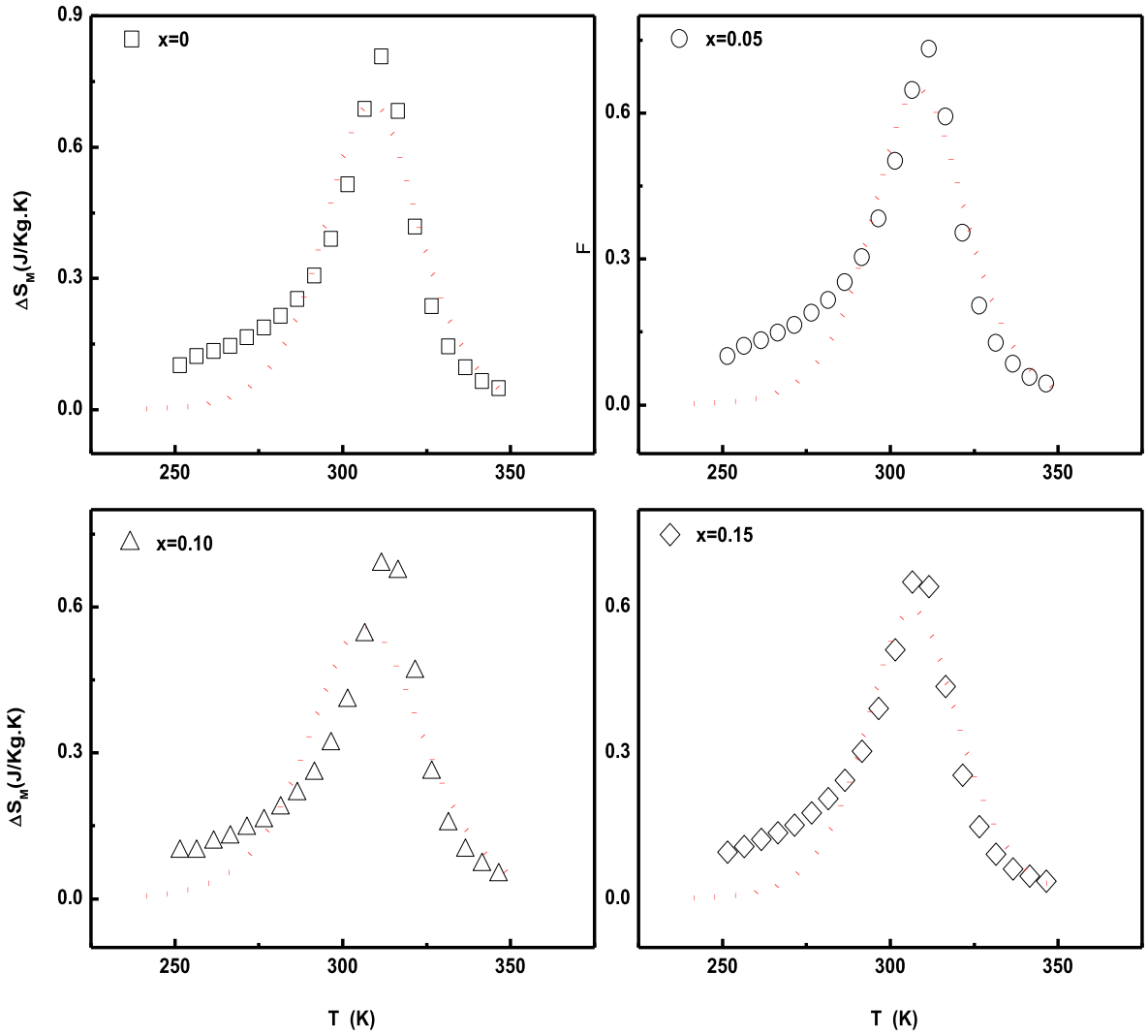

Fig. 9. Comparison between the experimental (symbols) and the calculated (dash lines) Magnetic entropy change, ($-\Delta S_M$), versus temperature for LSCMO sample at 0.5 T magnetic field.

Table 3
Parameters estimated from the best fit to Eq. (3) of the maximum entropy change $|\Delta S|_{max}$ curve of $(La_{0.70}Ba_{0.3}MnO_3)_{1-x}/(Al_2O_3)_x$ composite.

$(La_{0.70}Ba_{0.3}MnO_3)_{1-x}/(Al_2O_3)_x$	0	0.05	0.10	0.150
H(T)	0.5	0.5	0.5	0.5
M_i(emu g^{-1})	7.70	6.5	5.81	5.14
M_f(emu g^{-1})	0.79	0.41	0.311	0.433
B(emu g^{-1} K^{-1})	1.36×10^{-3}	1.9×10^{-3}	7.3×10^{-4}	5.1×10^{-4}
S_c (emu g^{-1} K^{-1})	−0.93149	−0.7289	−0.6316	−0.56433
ΔS_M(J Kg^{-1} K)	0.0465	0.0364	0.0315	0.0282
δT_{FWHM} (K)	8.06	11.58	13.48	11.23
RCP (J Kg^{-1})	33.38	42.21	42.57	31.69

(~98.77 Jkg^{-1} at $H = 2$ T) is approximately 65 percentage of that of pure Gd ($RCP = 153\ Jkg^{-1}$, $H = 2$ T). It means to achieve an active magnetic refrigerator employing LBMO will need more than one and half times the volumes of a refrigerant unit consisting of pure Gd.

Declaration of Competing Interest

The authors declare that they have no conflict of interest.

Acknowledgments

The authors would like thank Dr. Abd El-Moez A. Mohamed for his help on measuring the magnetocaloric effect.

References

[1] R. Yon Helmot, J. Wecker, B. Holzapfel, L. Schultz, K. Samwer, Phys. Rev. Lett. 71 (1993) 2331.
[2] G.H. Jonker, J.H. van Santen, Physica 16 (1950) 337.
[3] Y. Tokura, Singapore (2000) 1–52.
[4] H.F. Mohamed, J. Magn. Magn. Mater. 424 (2017) 44.
[5] L.I. Balcells, A.E. Carrilo, B. Martnez, J. Fontcuberta, Appl. Phys. Lett. 74 (1999) 4014.
[6] A.M. Ahmed, H.F. Mohamed, A.K. Diab, El-Moez A. Abd, Mohamed, A.E.A. Mazen, A.M. Mohamed, Indian J. Phys. 89 (2015) 561.
[7] M. Eshraghi, H. Salamati, P. Kameli, J. Alloy Compd. 437 (2007) 22.
[8] El-Moez A. Abd, Mohamed, Aml M. Mohamed, A. El Shafaie, H.F. Mohamed, A.K. Diab, A.M. Ahmed, Chem. Phys. Lett. 713 (2018) 272.
[9] A.M. Ahmed, H.F. Mohamed, A.K. Diab, Sara A. Mohamed, Indian J. Phys. 91 (2) (2017) 169.
[10] N.V. Khiem, P.T. Phong, N.V. Dai, H.D. Chinh, D.H. Manh, L.V. Hong, N.X. Phuc, Mater. Lett. 63 (2009) 899.
[11] D. Kumar, J. Sankar, J. Narayan, K. Singh Rajiv, A.K. Majumdar, Phys. Rev. B 65 (2002) 094407.
[12] J.C. Zhang, Y. Xu, S.X. Cao, G.X. Cao, Y.F. Zhang, C. Jing, Phys. Rev. B 72 (2005) 054410.
[13] E. Syskakis, G. Choudalakis, C. Papastaikoudis, J. Phys, Condens. Matter. 15 (45) (2003) 7735.

[14] H.F. Mohamed, A.M. Ahmed, A.K. Diab, Esraa Y. Omar, Chem. Phys. Lett. 726 (2019) 22.
[15] J. Fan, L. Ling, B. Hong, L. Pi, Y. Zhang, J. Magn. Magn. Mater. 321 (2009) 2838.
[16] P. Gorria, J.L.S. Llamazares, P. Álvarez, M.J. Pérez, J.S. Marcos, J. Phys. D: App. Phys. 41 (2008) 19.
[17] M.A. Hamad, J. Adv. Ceram. 1 (4) (2012) 290.
[18] G.K. Williamson, W.H. Hall, Acta Metall. Rgica 1 (1953) 22.
[19] K.D. Rogers, P. Daniels, Biomaterials 23 (12) (2002) 2577.
[20] K.S. Rao, B. Tilak, K.Ch.V. Rajulu, A. Swathi, H. Workineh, J. Alloys Compd. 509 (2011) 7121.
[21] J.A. Collado, C. Frontera, J.L. Garc'ia-Muñoz, C. Ritter, M. Brunelli, M.A.G. Aranda, Chem. Mater. 15 (2003) 167.
[22] P.M. Woodward, D.E. Cox, T. Vogt, C.N.R. Rao, A.K. Cheetham, Chem. Mater 11 (12) (1999) 3528.
[23] A. Llobet, C. Frontera, J.L. Garc'ia-Muñoz, C. Ritter, M.A.G. Aranda, Chem. Mater. 12 (12) (2000) 3648.
[24] G. Li, H.D. Zhou, S.L. Feng, X.J. Fan, X.G. Li, J. Appl. Phys. 92 (2002) 1406.
[25] S.K. Banerjee, Phys. Lett. 12 (1964) 16.
[26] E. Brück, O. Tegus, D.T.C. Thanh, K.H.J. Buschow, J. Magn. Magn. Mater. 310 (2007) 2793.